International Journal of Research and Technology in Electrical Industry

journal homepage: ijrtei.sbu.ac.ir

Shahid Beheshti University

Using Quadratic Inspired Optimization in Fuzzy Fractional Order PID Load Frequency Control of Microgrids with Motor Drive-based Load

Reza Nobari [1], Mohsen Hasan Babayi Nozadian[1,*], Mohamad Amin Ghasemi [1]

[1] *Department of Electrical Engineering, Faculty of Engineering, Bu-Ali Sina University, Hamedan, Iran*

ARTICLE INFO

Article history:
Received: 17 September 2025
Revised: 24 December 2025
Accepted: 04 January 2026

Keywords:
Microgrid
Fractional-order fuzzy pid
Quadratic inspired optimization
Motor drive-based load
Load frequency control

ABSTRACT

Microgrids operating in isolated mode often suffer from frequency instability due to unpredictable load variations and intermittent renewable energy generation. This paper proposes an enhanced load frequency control strategy that combines fuzzy logic with fractional-order PID dynamics to address these challenges. The fuzzy inference mechanism generates a nonlinear control action based on frequency deviation and its rate of change, enabling real-time, intelligent adaptation to disturbances. Fractional-order operators enhance damping and robustness across a wide operating range.

Controller parameters are tuned using a Quadratic Inspired Optimization (QIO) algorithm to minimize performance indices like Integral Absolute Error (IAE) and Integral Time Absolute Error (ITAE). A key innovation is incorporating motor drive-based loads as controllable frequency-responsive elements, rather than mere disturbances. Despite their nonlinear nature, these loads are harnessed to boost dynamic performance and accelerate stabilization.

MATLAB/Simulink simulations across scenarios—consumer loads only, renewables only, and combined—confirm the strategy reduces frequency deviations and improves transient performance over PID, FOPID, and fuzzy-based benchmarks, with superior error metrics and recovery times. This highlights the method's robustness for real-world microgrids.

1. Introduction

A microgrid is a system composed of multiple distributed generation sources and energy storage resources, managed through power electronic devices such as inverters and rectifiers. Microgrids can operate either in grid-connected mode or in islanded mode [1, 2]. Most power systems are made up of several areas that generate energy to meet load demands. However, mismatches between generated energy and consumed load can cause deviations in the system frequency from its nominal value, violating power quality standards. These aspects highlight the importance of Load Frequency Control (LFC) in power systems [3, 4].

Various methods of load frequency control (LFC) have been examined and evaluated for microgrids using both conventional and modern approaches across different references. In [5], an adaptive load-frequency control method is presented for islanded two-area power systems using an integral controller. Similarly, [6] adjusts the integral controller gain online using Electric Search Optimization (ESO) and the Balloon Effect, supported by an optimized Jaya algorithm. In [7], a PI-PD controller is applied to hybrid systems, with Reduced Hankel Matrix modelling and PSO-GSA optimization. In [8], a dual-mode PI-PD controller is proposed for systems combining renewable and conventional power sources. The effectiveness of classical PID control is further explored

* Corresponding author
E-mail address: m.nozadian@basu.ac.ir
https://orcid.org/0000-0002-0225-7059
https://dx.doi.org/10.48308/ijrtei.2026.241506.1101

in [9], which analyses DFIG-based wind systems, and in [10], which employs the Black Widow Optimization Algorithm (BWOA) for PID parameter tuning in systems integrating thermal and photovoltaic sources. In [11], a PID controller with three degrees of freedom (DOF) is optimized using the Seagull Optimization Algorithm (SOA) in a multi-area system containing thermal, hydro, and nuclear generators.

Efforts to improve robustness and adaptability have led to more complex designs. In [12], the Modified African Buffalo Optimization (MABO) is used to tune multiple PID variants and is benchmarked against other swarm-based methods. In [13], a self-tuning PID controller updates its parameters in real time, while [14] introduces sliding mode control with a decentralized disturbance observer for managing external disturbances. A delay-tolerant H∞ controller is implemented in [15] for robust regulation in interconnected systems. A shift toward predictive and AI-based strategies appears in [16], which uses model predictive control (MPC) for tidal, diesel, and electric vehicle coordination in islanded hybrid power systems. Similarly, [17] integrates generalized active disturbance rejection control (GADRC), while [18] applies a neural network internal model control (NNIMC) scheme in large-scale systems. Attention to cybersecurity is given in [19], which explores defence mechanisms against false data injection attacks (FDIA) using fuzzy logic and neural networks. Fuzzy and intelligent controllers show significant promise. In [20], ANFIS is used for hydropower AGC, unlike [21], which focuses on an ANFIS/FOPID-based framework with observer-assisted design in a different system context, the present work targets isolated microgrids and emphasizes explicit MDL participation in the frequency control loop combined with QIO-based tuning. In [22], a fractional-order PID fuzzy controller (FOFPID) manages multi-source systems under sudden load changes. A type-2 fuzzy PID tuned by modified equilibrium optimization is proposed in [23], and [24] introduces an IT2 fuzzy fractional-order PD-PI controller optimized via the Cheetah Optimizer for islanded microgrid stability.

More refined hybrid controllers continue this trend. In [25], a novel SIT2-FLC with fractional-order gradient descent (FGD) manages a tidal/V2G hybrid islanded microgrid. In [26], a type-2 fuzzy controller replaces type-1 fuzzy PID for better secondary control in hybrid systems.

To further this progression, recent works [27] and [28] propose hybrid and fractional-order intelligent controllers, such as the TIDF-HYBFO combination and the FOI-TDN controller optimized with sinusoidal-cosine algorithms. Reference [29] uses VIC-based hybrid optimization, while [30] builds on this with a fuzzy-based self-adaptive triple-loop control to dynamically adjust inertia in RES-based systems. In [31], a high-order fractional controller is proposed with differential feedback, showcasing advanced dynamic control potential in multi-area systems. Through this steady evolution from basic integral control to intelligent and adaptive fuzzy fractional-order designs there is a clear trend toward more resilient, precise, and adaptable controllers. These trends converge toward controllers that can combine fuzzy intelligence with fractional calculus, offering a higher degree of flexibility and robustness particularly relevant in motor-drive-based load frequency control strategies for modern microgrids.

The integration of RESs like wind and solar creates frequency stability challenges in islanded microgrids, especially when combined with motor drive-based loads (MDLs), which exhibit fast nonlinear dynamics. While traditionally seen as disturbances, MDLs can enhance system stability if properly utilized. Recent studies show that advanced controllers such as MPC, GSMDC, and hierarchical methods, alongside leveraging motor inertia, can reduce reliance on costly BESS [24].

Despite recent ongoing progress, many LFC methods still fall short under highly dynamic, uncertain conditions. This study proposes a fuzzy fractional-order PID controller, optimized via a quadratic-inspired algorithm, that actively incorporates MDL dynamics offering improved stability and positioning MDLs as assets rather than liabilities in microgrid control. Adaptive strategies have been proposed to control motor drive-based loads using model predictive control (MPC), leveraging both mechanical and electrical inertia in variable speed drives (VSDs) to aid frequency regulation. While effective, such methods often depend heavily on precise system modelling and tuning, limiting their adaptability under nonlinear and uncertain conditions common in microgrids [32]. Other studies have proposed retrofitting motor drive loads with grid-supporting controllers to achieve fast primary-frequency response, demonstrating sub-100 ms reaction times comparable to battery systems. However, these approaches rely on reduced-order models and fixed control parameters, which may limit scalability and adaptability in more complex or disturbance-prone microgrids [33].

To address these research gaps, this paper presents an integrated LFC approach for isolated microgrids that synergizes fuzzy logic and tuning the controller parameters with a fractional-order PID structure, optimized via the Quadratic Inspired Optimization (QIO) algorithm. Unlike many existing strategies that either exclude motor drive-based loads (MDLs) from the control loop or treat them merely as external disturbances, this study explicitly incorporates MDL dynamics into the microgrid's frequency response model. For the LFC analysis, MDLs are represented using standard first-order equivalent models (CT, CP, and CS modes). This approach ensures that the dominant frequency-relevant dynamics are captured while keeping the overall system model computationally tractable for robust controller design.

The main contribution of this paper is an integrated LFC framework that combines: (i) explicit inclusion of MDL dynamics (CT/CP/CS modes) within the isolated microgrid model, (ii) a fractional-order fuzzy PID (FOFPID) control structure suitable for the considered microgrid dynamics, and (iii) offline QIO-based tuning of the controller parameters using ITAE/IAE performance objectives under multiple operating scenarios.

The rest of this paper is organized as follows: Section 2 presents the mathematical modelling of MG components, including generation sources, storage systems, and MDLs. Section 3 describes the controller design, covering FOPID, fuzzy logic integration, and QIO-based tuning.

Section 4 reports the simulation results and performance analysis under various operating conditions. Section 5 concludes the paper.

2. Modelling of the Microgrid

The isolated microgrid under study incorporates a diverse range of distributed generation resources—including diesel engine generators, photovoltaic systems, wind turbine generators, aqua electrolyzers, and fuel cells—alongside energy storage systems such as electric vehicles (EVs), flywheel energy storage systems (FESS), and battery energy storage systems (BESS). Additionally, motor drive-based loads (MDLs) are explicitly integrated into the control framework. In LFC studies, the primary focus is on the aggregate power-frequency response and electromechanical oscillations rather than high-frequency electromagnetic transients. Therefore, representing MDLs via first-order equivalent models is both appropriate and sufficient to capture the dominant frequency-relevant dynamics while ensuring the stability analysis remains computationally efficient for controller synthesis. The dynamic models of these components are detailed below and illustrated in Fig. 1 [29, 30].

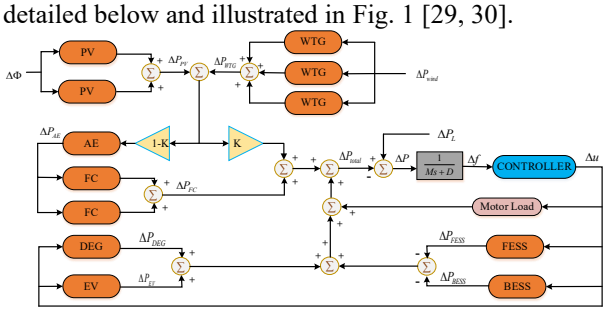

Fig. 1. Structure of an Islanded Microgrid

2-1- Diesel Engine Generator (DEG)

Generally, diesel engine generators are integrated into microgrid systems with renewable energy sources (RES) to provide backup power due to the intermittent nature of RES [1]. In the event of a sudden increase in load demand, the dynamic response of the diesel generator ensures that the system's power requirements are met. The commonly used dynamic model of diesel generator for LFC studies is as presented through (1) [7]. These simplified models enable integration of the diesel generator into system-level simulations and control design by capturing its essential dynamic characteristics without relying on complex physical modelling.

where the transfer function of the diesel generator considers its gain and time constant, with K_{DEG} and T_{DEG} representing the gain and time constant, respectively, of the first-order transfer function characterizing the dynamic behaviour of the diesel generator.

$$G_{DEG}(s)=\frac{K_{DEG}}{1+sT_{DEG}} \tag{1}$$

2-2- Wind Turbine Generator (WTG)

The wind turbine generators system exhibits nonlinear characteristics, including a pitch control system. One notable feature of wind turbines is the adjustment of the pitch angle in response to wind speed changes, which introduces nonlinearity [30]. However, the studies where WTG are just injecting their intermittent power to grid and not participating in frequency control, it can be modelled using (2) [7]. These simplified models enable integration of the wind turbine generator (WTG) into system-level simulations and control design by capturing its essential dynamic characteristics without the need for complex physical modelling, where K_{WTG} and T_{WTG} represent the gain and time constant, respectively, of the WTG's first-order transfer function.

$$G_{WTG}(s)=\frac{K_{WTG}}{1+sT_{WTG}} \tag{2}$$

2-3- Photovoltaic (PV)

The photovoltaic (PV) is integrated into the system as a renewable energy source and is highly dependent on ambient temperature and solar irradiance [1,8]. The PV generator is modelled using (3), these simplified models enable integration of the photovoltaic (PV) generator into system-level simulations and control design by capturing its essential dynamic characteristics without the need for complex physical modelling, where K_{PV} and T_{PV} represent the gain and time constant of the PV generator's first-order transfer function [8].

$$G_{PV}(s)=\frac{K_{PV}}{1+sT_{PV}} \tag{3}$$

2-4- Energy Storage Systems

$$G_{BESS}(s)=\frac{K_{BESS}}{1+sT_{BESS}} \tag{4}$$

$$G_{FES}(s)=\frac{K_{FESS}}{1+sT_{FESS}} \tag{5}$$

$$G_{EV}(s)=\frac{K_{EV}}{1+sT_{EV}} \tag{6}$$

In these expressions, K and T denote the gain and time constant of each storage unit, respectively. For batteries (4), K_{BESS} and T_{BESS} represent the battery's efficiency and charge/discharge time constant. Similarly, K_{FESS} and T_{FESS} in Equation (5) correspond to the gain and dynamic response of the flywheel energy storage system. Equation (6) models' electric vehicles (EVs) acting as storage units, where K_{EV} and T_{EV} characterize the energy exchange efficiency and response time of the EV's power electronics.

2-5- Electrolyzer and Fuel Cell

Electrolyzers and fuel cells are integrated into microgrids to support energy conversion and storage in hybrid renewable energy systems. Their dynamic behaviour can be effectively captured using first-order transfer functions that relate input pressure changes to output power response.

The transfer function of the electrolyzer is expressed as (7),

$$G_{AE}(s)=\frac{K_{AE}}{1+sT_{AE}} \quad (7)$$

Similarly, the fuel cell system is modelled as (8) as follows:

$$G_{FC}(s)=\frac{K_{FC}}{1+sT_{FC}} \quad (8)$$

In these models, K_{AE} and T_{AE} denote the gain and time constant of the electrolyzer system, respectively, reflecting its power response to pressure variations. Likewise, K_{FC} and T_{FC} represent the dynamic response parameters of the fuel cell. These simplified models enable integration of the AE and FC units into system-level simulations and control design by capturing their essential dynamic characteristics without the need for complex physical modelling.

2-6- MDL

MDLs are a critical component of modern microgrids, particularly in industrial and commercial environments where they directly affect system dynamics. Unlike traditional passive loads, MDLs are connected via power electronic interfaces, which allow for fast, nonlinear, and time-varying behaviour. To represent their impact on frequency control, this study categorizes MDLs into three representative operating modes: constant torque (CT), constant power (CP), and constant speed (CS). These categories reflect typical mechanical load characteristics observed in real-world applications such as conveyors, machining systems, and centrifugal equipment. Each mode is modelled using a first-order transfer function, denoted respectively as G_{CT}, C_{CP}, and G_{CS}, where the gain and time constant define the response of the load to system changes. The CT load maintains fixed torque regardless of speed variation, while the CP load keeps power constant with torque and speed adjusting inversely. In CS loads, speed remains fixed, and torque varies with demand. These simplified models offer a practical way to include MDLs in control system design and allow for realistic analysis of their effect on frequency stability under various operating scenarios. Table 1 presents the power rating, time constant, and dynamic gain of various microgrid sources, which are used to model their behaviour in response to power variations.

$$G_{CT}(s)=\frac{KCT}{1+sT_{CT}} \quad (9)$$

$$G_{CP}(s)=\frac{K_{CP}}{1+sT_{CP}} \quad (10)$$

$$G_{CS}(s)=\frac{K_{CS}}{1+sT_{CS}} \quad (11)$$

In this study, the parameters for the MDL equivalent models are selected to reflect representative fast electrical-drive dynamics relevant to the LFC time scale. The specific parameter values utilized in the simulations are as follows:

CT mode: $K_{CT}=0.5$, $T_{CT}=0.7$
CP mode: $K_{CP}=0.75$, $T_{CP}=1$
CS mode: $K_{CS}=1$, $T_{CS}=0.6$

These values are kept consistent across all test scenarios to ensure a fair and rigorous comparison of controller performance, while the transitions between operating modes demonstrate the resulting changes in the effective power-frequency response characteristics.

Table 1. Values for various parameters of the MG

Type of the MG Resources	Gain value	Time constant
WT	1	1.5
PV	1	0.03
BESS	1.8	0
FESS	0.098	0.03
DEG_1 & DEG_2	1	0.5
AE_1 & AE_2	1	0.05
FC_1 & FC_2	1	3

AE1/AE2 and FC1/FC2 denote the electrolyzer and fuel-cell units shown in Fig. 1, where identical parameter settings are assigned to each corresponding pair.

3. Controller Design

This section presents the control design used for load frequency control of the isolated microgrid. The proposed controller combines fuzzy logic with fractional-order PID dynamics to improve damping and robustness under renewable intermittency and motor-drive load variations. For benchmarking, the proposed controller is compared against conventional PID, FOPID, and a fuzzy-based fractional benchmark controller under the same operating scenarios. A centralized control structure is considered, where a unified control signal is distributed across the participating resources.

3-1- FOPID Controller Design

This subsection briefly presents the fractional-order PID (FOPID) controller used as a baseline and as a building block for the proposed structure. Fractional calculus extends classical PID control by allowing non-integer integration and differentiation orders. Fractional calculus extends classical calculus to non-integer orders. The Caputo fractional derivative and the fractional integral are two common definitions used in control systems. The corresponding expressions are shown in (11) and (12) [34, 35].

$$D_t^a f(t)=\frac{1}{\Gamma(n-a)}\int(t-\tau)^{a-n+1}f^n(\tau)d\tau \quad (11)$$

$$I_t^a f(t)=\frac{1}{\Gamma(a)}\int(t-\tau)^{a-1}f(\tau)d\tau=D_{0,t}^{-a}f(t) \quad (12)$$

The control signal generated by the fractional-order PID (FOPID) controller is defined as:

$$G(s)=K_P+K_D s^{\mu}+\frac{K_I}{s^{\lambda}} \quad (13)$$

In this expression, K_P, K_I, and K_D represent the proportional, integral, and derivative gains, respectively.

The parameters λ and μ denote the fractional orders of integration and differentiation. When $\lambda = \mu = 1$, the equation simplifies to the classical PID control law.

3-2- Fuzzy Controller Implementation

This work adopts a fractional-order fuzzy PID (FOFPID) structure, where a fuzzy PID generates the control action based on the frequency deviation e and its rate $\dot{e}$, and fractional-order operators are applied to enhance dynamic flexibility and damping. In this formulation, fuzzy inference provides a nonlinear rule-based control action, while the fractional dynamics improve robustness; the controller parameters are tuned offline using QIO.

The membership functions are designed using a normalized input range. The error e and its rate $\dot{e}$ are scaled by input gains so that both signals lie within comparable normalized bounds under expected operating conditions. Five symmetric linguistic terms (LN, SN, ZE, SP, LP) are then placed uniformly over this normalized range with overlap to provide smooth rule transitions. The same term set is used for e and $\dot{e}$ to keep the rule base compact and interpretable; differences in physical units and typical magnitudes are handled by the scaling gains rather than by using different linguistic partitions [36, 37].

The fuzzy logic controller acts as an intelligent decision-making system that tunes the control signal based on observed error and its rate of change. The fuzzy controller receives two inputs: the system error $e(t)$ and the fractional derivative of the error $\dot{e}(t)$. Each of these inputs, as well as the output, is defined over five linguistic variables: LN (large negative), SN (small negative), ZE (zero), SP (small positive), and LP (large positive). These variables are associated with triangular and trapezoidal membership functions, as shown in Fig. 2. The membership functions map numerical input values to degrees of membership in fuzzy sets, enabling smooth transitions between control actions. Overlapping membership functions are used to ensure smooth transitions between adjacent rule outputs and to avoid abrupt control changes [36, 37].

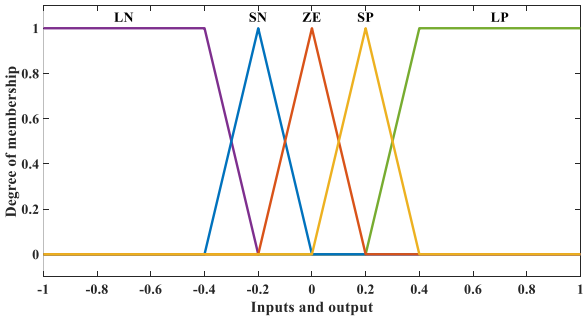

Fig. 1. Fuzzy logic membership functions

Table 2. Fuzzy Rules

e(t) / ė (t)	LN	SN	ZE	SP	LP
LP	ZE	SP	LP	LP	LP
SP	SN	ZE	SP	LP	LP
ZE	LN	SN	ZE	SP	LP
SN	LN	LN	SN	ZE	SP
LN	LN	LN	LN	SN	ZE

The rule base of the fuzzy controller consists of 25 if-then rules, constructed based on expert knowledge of system behaviour. These rules determine the controller's output based on the combination of $e(t)$ and $\dot{e}(t)$, each mapped to one of the five linguistic terms. The rule matrix is presented in Table 2. For instance, if $e(t) = LP$ and $\dot{e}(t) = SP$, the output is ZE, indicating that only minor correction is needed. Conversely, if both inputs are LN, the output is also LN, signalling the need for aggressive corrective action. This rule set ensures that the controller reacts appropriately to both the magnitude and the rate of error, allowing adaptive response to dynamic operating conditions.

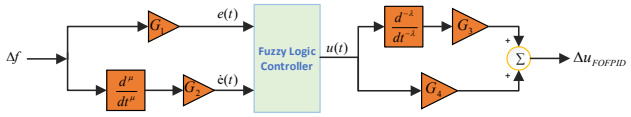

Fig. 3. The proposed control system structure

The complete control structure of the FOFPID controller is illustrated in Figure 3. The error signal Δf and its fractional derivative are scaled and fed into the fuzzy logic controller, which generates an intermediate control signal $u(t)$. This signal is then passed through a fractional integrator and differentiator block, followed by gain scaling elements, to produce the final control output Δu_{FOFPID}. The design allows both intelligent decision-making through fuzzy logic and fine-tuned dynamic shaping via fractional-order elements, forming a hybrid controller capable of managing complex, nonlinear system dynamics with high precision.

3-3- Quadratic Inspired Optimization Algorithm

To precisely tune the parameters of the proposed FOFPID controller for managing frequency deviations in the microgrid, a Quadratic Interpolation Optimization (QIO) algorithm is employed. This algorithm is based on the Generalized Quadratic Interpolation (GQI) method and offers strong capabilities in both global and local search. The objective function used in the optimization is the Integral of Time-weighted Absolute Error (ITAE), which minimizes the frequency error over time while enhancing the overall stability of the system. Candidate parameter sets that produce unstable or non-convergent simulations are rejected by assigning a large penalty value to the objective function (14),

$$J = J_{\mathrm{ITAE}} + \Pi, \text{ where } \Pi = M \tag{14}$$

if the simulated frequency deviation diverges or does not settle within the simulation horizon, and$\Pi = 0$ otherwise. This ensures that the optimizer searches only within the practically stable parameter region while minimizing the performance index. The controller parameters, including scaling gains G_1 to G_4 and fractional orders λ and μ, are optimized within predefined bounsds. The optimization aims to improve system stability under varying load conditions and to reduce control signal oscillations. The QIO process involves generating an initial random population, performing global and local searches, and

iterating the process until the optimal parameter set is identified. This approach ensures that the FOFPID controller maintains robustness and energy efficiency in highly dynamic microgrid environments. Several metaheuristic optimizers have been used for LFC tuning in related work, including PSO, GA, DE, and hybrid strategies. QIO is selected here because its generalized quadratic interpolation mechanism provides an efficient balance between exploration and exploitation with relatively few tuning parameters compared with many swarm-based methods. This can improve convergence reliability for multi-parameter controllers such as fractional-order structures, while keeping the optimization setup straightforward for practical controller tuning [34].

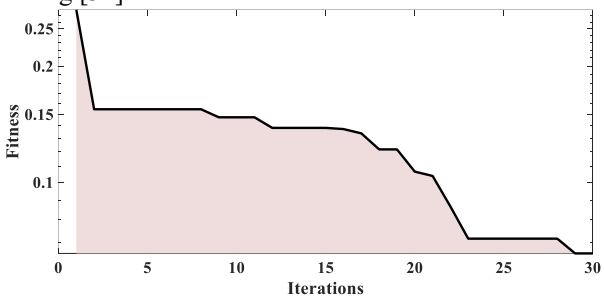

Fig. 4. Fitness curve of the QIO algorithm during parameter optimization

The convergence behaviour of the QIO algorithm is illustrated in Figure 4. The fitness value, which represents the value of the objective function (ITAE), consistently decreases over 30 iterations, indicating effective parameter tuning. The sharp initial decline followed by gradual improvements reflects the balance between global exploration and local exploitation phases of the algorithm. This trend confirms that the QIO method successfully identifies an optimal parameter set for the FOFPID controller, minimizing frequency deviation while maintaining robust system performance which are subsequently shown as the optimized parameters in Table 3.

Table 3. The control parameters.

Terms	Value
G_1	0.8129
G_2	0.76123
G_3	82.53
G_4	98.1971
μ	0.8121
λ	0.9918

Regarding real-time implementation, QIO-based tuning is performed offline, and only the resulting fixed controller parameters are used online. The real-time computation therefore reduces to fuzzy inference (rule evaluation and defuzzification) plus the controller's transfer-function operations, which are feasible on common microgrid controllers (DSP/PLC/industrial embedded platforms). Fractional-order operators can be implemented using standard rational approximations within the frequency band of interest, enabling deployment without excessive computational burden [38].

4. Results and Simulations

This section presents and analyses the simulation results to evaluate the impact of MDLs on LFC performance in microgrids. We begin by comparing the system's frequency response in two cases: with and without MDLs. This comparison highlights the influence of MDLs on frequency deviations and control effort. Following this, three simulation scenarios are considered to reflect different operating conditions. In Scenario 1, only consumer loads are active. Scenario 2 involves only RESs, with no consumer loads present. Scenario 3 includes both consumer loads and RESs simultaneously. These scenarios aim to provide a comprehensive understanding of how MDLs interact with varying microgrid configurations in terms of frequency control behaviour.

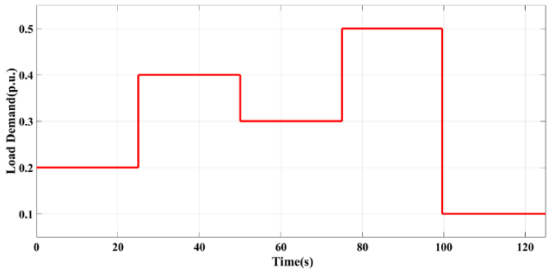

Fig. 5. Load variations over time.

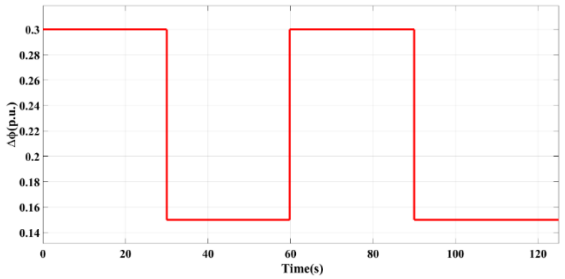

Fig. 6. Variations in solar irradiance intensity over time.

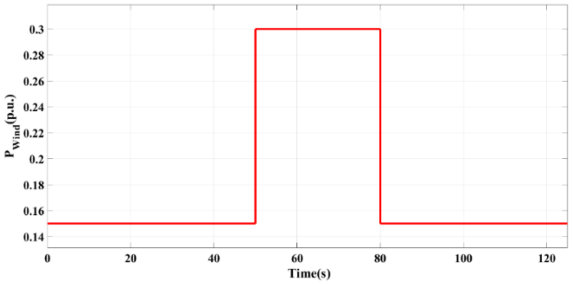

Fig. 7. Variations in wind power output over time.

The variations in electrical load and the input profiles applied to the RESs namely the photovoltaic generator and wind turbine are illustrated in Figures 5–7. These figures show the changes in solar irradiance, wind power, and load demand, all based on realistic weather and consumption conditions typically observed in microgrids.

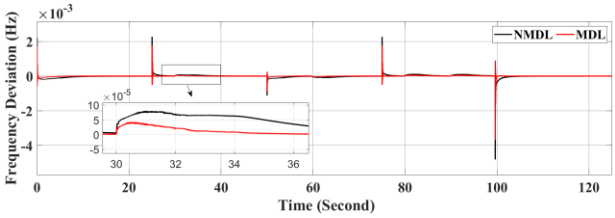

Fig. 8. Comparison of the Impact of Motor Drive-Based Loads on Frequency Deviations

Fig. 8 presents a comparison of the system's frequency deviations in the presence and absence of motor drive-based loads. Two cases are considered: one with MDLs (labelled MDL) and the other without MDLs (labelled NMDL). The horizontal axis represents time (in seconds), while the vertical axis shows frequency deviation (in Hz). As observed, the inclusion of MDLs introduces slight changes in system frequency, which appear as small deviations from the nominal frequency level. These subtle shifts highlight the dynamic influence of MDLs on frequency behaviour in microgrid environments.

4-1- Scenario 1:

In the first scenario, the microgrid operates solely with consumer loads, without any contribution from renewable energy sources or motor drive-based loads. This setup serves as a baseline to evaluate the controller's performance in handling conventional load fluctuations. The goal is to assess how well the system maintains frequency stability under demand-side disturbances and whether it can respond effectively to sudden changes in load while preserving operational integrity.

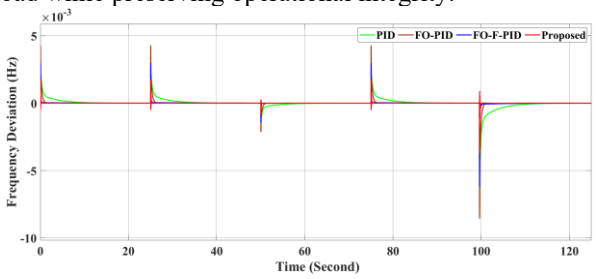

Fig. 9. Comparison between the proposed approach and selected reference methods under Scenario 1 (consumer loads only).

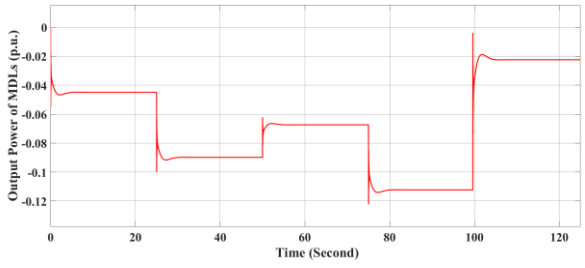

Fig. 10. MDLs output power

Fig. 9 provides an additional view comparing the performance of four control strategies: PID, FO-PID, FO-F-PID, and the proposed method. This comparison is presented over a shorter time interval (less than 1.5 seconds) for Scenario 1 (consumer loads only). As evident from the figure, the proposed method reduces the peak frequency deviation and suppresses oscillations more effectively than the other approaches, yielding improved transient regulation following load changes. These results highlight the effectiveness of the proposed method in minimizing transient frequency oscillations and ensuring system stability in response to sudden load changes. The output power of MDLs in scenario I is shown in Fig. 10. Fig. 11 presents the same comparison with a slightly more zoomed-in view to further emphasize the early-stage dynamic behaviour of each method. To better illustrate the transient, undershoot differences at nonzero peak instants, an additional magnified view around the highlighted peak interval is provided.

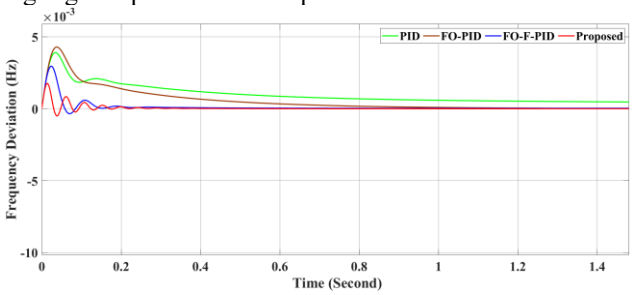

Fig. 11. A closer view of the comparison between the proposed method and selected reference approaches in Scenario 1.

4-2- Scenario 2:

In this scenario, the system is simulated under conditions where renewable energy sources such as wind turbines and photovoltaic panels are the sole providers of power. No consumer loads are present, allowing for isolated analysis of the system's frequency regulation when driven entirely by variable generation. The key characteristics of this scenario include fluctuations in power generation caused by changing environmental conditions (such as wind speed and solar irradiance), challenges in maintaining frequency stability due to the intermittent nature of RESs, and an overall assessment of the system's ability to remain stable in the absence of consumer demand.

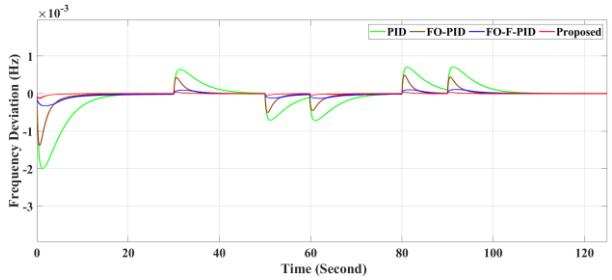

Fig. 12. Comparison between the proposed method and selected reference approaches in Scenario 2.

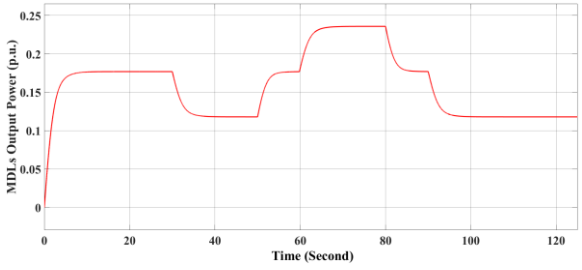

Fig. 13. MDLs power output in Scenario II

Fig. 12 compares the performance of PID, FO-PID, FO-F-PID, and the proposed method under Scenario 2, where RESs are the only power sources. The time axis is in seconds, and the vertical axis shows frequency deviation in Hz. The proposed method demonstrates reduced deviation amplitude and less oscillatory behaviour than the other strategies, indicating improved frequency regulation under renewable generation variability. These results highlight its effectiveness in managing renewable generation fluctuations and maintaining system stability without consumer loads. The output power of MDLs in scenario II is shown in Fig. 13.

4-3- Scenario 3:

In this scenario, the system is modelled with a simultaneous combination of RESs and consumer loads. The aim is to examine the interaction between renewable generation and demand-side variability, assess the impact of both production and load fluctuations on frequency stability, and evaluate the controller's performance in managing this complex dynamic environment.

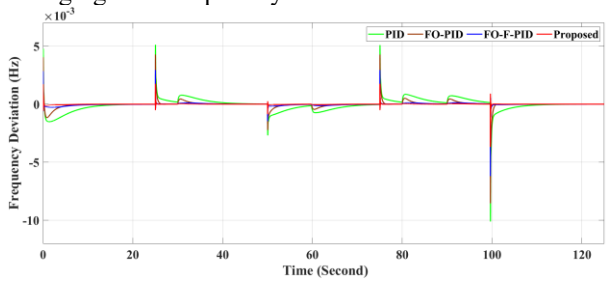

Fig. 14. Comparison between the proposed method and selected reference approaches in Scenario 3.

Fig. 14 presents the overall system response to the combined effect of consumer loads and RESs under Scenario 3. The proposed method shows improved performance in minimizing frequency deviations and delivering a more stable response compared to the other control strategies. Fig. 15 provides a zoomed-in view of the same comparison, highlighting differences in peak deviation and oscillation decay among the controllers. The output power of MDLs in scenario III is shown in Fig. 16. Table4, 5 and 6 show the IAE and ITAE comparison between the proposed and similar methods. To better illustrate the transient, undershoot differences at nonzero peak instants, an additional magnified view around the highlighted peak interval is provided.

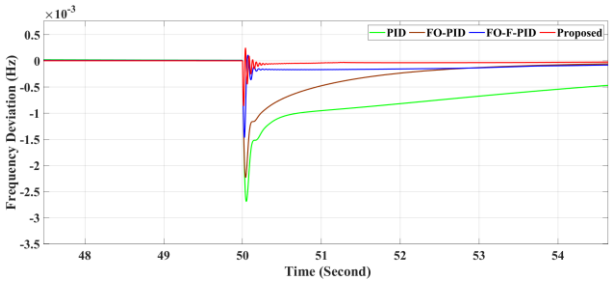

Fig. 15 A closer view of the comparison between the proposed method and selected reference approaches in Scenario 3.

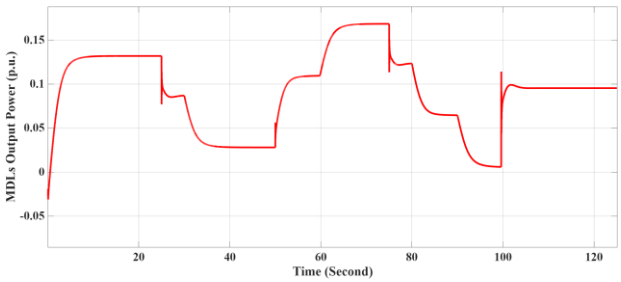

Fig. 16. MDLs power output in Scenario III

In Table4, 5 and 6 quantitative evaluations using ITAE and IAE metrics showed significant improvements up to 98.28% in ITAE and 85.66% in IAE compared to FO-F-PID that has the closest structure to the proposed control method, demonstrating the method's effectiveness in maintaining frequency stability under varying operating conditions

Table 4. IAE and ITAE comparison

Comparison method		
Method	ITAE	IAE
Proposed	0.03406	0.0005521
FO-F-PID	0.157	0.002491
FO-PID	0.3311	0.005522
PID	1.071	0.0173

Table 5. IAE and ITAE comparison

Comparison method		
Method	IAE	ITAE
Proposed	0.03853	0.0009285
FO-F-PID	0.006171	0.263
FO-PID	0.01025	0.4212
PID	0.03295	1.428

Table 6. IAE and ITAE comparison

Comparison method		
Method	IAE	ITAE
Proposed	0.095	0.001921
FO-F-PID	0.3663	0.007296
FO-PID	0.7107	0.01394
PID	2.357	0.04365

5. Conclusion

This study addressed load frequency control in isolated microgrids with high renewable penetration and motor drive-based loads. A control strategy that explicitly includes MDL dynamics and applies a FOFPID structure tuned by the quadratic-inspired QIO algorithm was evaluated under three operating scenarios. Simulation results demonstrate that the proposed method reduces frequency deviation and improves overall transient regulation performance compared with PID, FOPID, and FO-F-PID benchmark controllers. Quantitative comparisons using IAE and ITAE (Tables 4 - 6) confirm substantial performance gains across all scenarios, achieving reductions of up to 98.28% in ITAE and 85.66% in IAE relative to the FO-F-PID approach, which is structurally the most comparable. These reductions in IAE and ITAE, along with the presented transient responses, indicate improved settling times (due to ITAE's emphasis on time-weighted errors) and enhanced system stability under diverse operating conditions.

Future work will focus on experimental validation, including hardware-in-the-loop testing and implementation on a real-time microgrid control platform to evaluate computational requirements, measurement noise sensitivity, and practical actuator constraints.

6. References

[1] M. Ali *et al.*, "Design of cascaded PI-fractional order PID controller for improving the frequency response of hybrid microgrid system using gorilla troops optimizer," *IEEE Access*, vol. 9, pp. 150715–150732, 2021.

[2] E. Tsybina, C. Winstead, B. Ollis, M. Olama, T. Kuruganti, "Demand response for frequency regulation: Research continuity and knowledge gaps," *Renewable and Sustainable Energy Reviews*, vol. 207, 114958, 2025.

[3] K. B. Meziane, R. Naoual, and I. Boumhidi, "Type-2 fuzzy logic based on PID controller for AGC of two-area with three source power system including advanced TCSC," *Procedia Computer Science*, vol. 148, pp. 455–464, 2019.

[4] H. Shayeghi, A. Rahnama, and H. H. Alhelou, "Frequency control of fully-renewable interconnected microgrid using fuzzy cascade controller with demand response program considering," *Energy Reports*, vol. 7, pp. 6077–6094, 2021.

[5] T. H. Mohamed, M. A. M. Alamin, and A. M. Hassan, "A novel adaptive load frequency control in single and interconnected power systems," *Ain Shams Engineering Journal*, vol. 12, no. 2, pp. 1763–1773, 2021.

[6] Y. A. Dahab, H. Abubakr, and T. H. Mohamed, "Adaptive load frequency control of power systems using electro-search optimization supported by the balloon effect," *IEEE Access*, vol. 8, pp. 7408–7422, 2020.

[7] V. Veerasamy *et al.*, "A Hankel matrix based reduced order model for stability analysis of hybrid power system using PSO-GSA optimized cascade PI-PD controller for automatic load frequency control," *IEEE Access*, vol. 8, pp. 71422–71446, 2020.

[8] M. K. Debnath, S. K. Kar, and S. Tripathy, "Optimal design of PI/PD dual mode controller based on quasi opposition-based learning for power system frequency control," *Adv. Electr. Eng. Electron. Energy*, vol. 4, p. 100135, 2023.

[9] S. Chaine and M. Tripathy, "Performance of CSA optimized controllers of DFIGs and AGC to improve frequency regulation of a wind integrated hydrothermal power system," *Alexandria Engineering Journal*, vol. 58, no. 2, pp. 579–590, 2019.

[10] P. Dahiya and A. K. Saha, "Frequency regulation of interconnected power system using black widow optimization," *IEEE Access*, vol. 10, pp. 25219–25236, 2022.

[11] C. N. S. Kalyan and C. V. Suresh, "Higher order degree of freedom controller for load frequency control of multi area interconnected power system with time delays," *Global Transitions Proceedings*, vol. 3, no. 1, pp. 332–337, 2022.

[12] B. Singh *et al.*, "An application of nature inspired algorithm based dual-stage frequency control strategy for multi micro-grid system," *Ain Shams Engineering Journal*, vol. 14, no. 9, p. 102125, 2023.

[13] N. Hasan *et al.*, "Robust self-tuned AGC controller for wind energy penetrated power system," *Ain Shams Engineering Journal*, vol. 13, no. 4, p. 101663, 2022.

[14] F. Farivar, O. Bass, and D. Habibi, "Decentralized disturbance observer-based sliding mode load frequency control in multiarea interconnected power systems," *IEEE Access*, vol. 10, pp. 92307–92320, 2022.

[15] S. K. Pradhan and D. K. Das, "H∞ load frequency control design based on delay discretization approach for interconnected power systems with time delay," *J. Mod. Power Syst. Clean Energy*, vol. 9, no. 6, pp. 1468–1477, 2020.

[16] A. Kumar *et al.*, "Load frequency control of distributed generators assisted hybrid power system using QOHSA tuned model predictive control," *IEEE Access*, vol. 10, pp. 109311–109325, 2022.

[17] S. Chang and S. Qi, "Design and analysis of a load frequency control system based on improved artificial intelligence control algorithm," *Alexandria Engineering Journal*, vol. 61, no. 12, pp. 11779–11786, 2022.

[18] N. Kumar *et al.*, "Novel neural network-based load frequency control scheme: a case study of restructured power system," *IEEE Access*, vol. 9, pp. 162231–162242, 2021.

[19] Z. Chen *et al.*, "Detection of false data injection attacks on load frequency control system with renewable energy based on fuzzy logic and neural networks," *J. Mod. Power Syst. Clean Energy*, vol. 10, no. 6, pp. 1576–1587, 2022.

[20] T. Weldcherkos, A. O. Salau, and A. Ashagrie, "Modeling and design of an automatic generation control for hydropower plants using neuro-fuzzy controller," *Energy Reports*, vol. 7, pp. 6626–6637, 2021.

[21] H. Maleki, S. Shirali, and H. Delavari, "Adaptive neuro-fuzzy fractional load frequency control via neural network observer," in *Proc. 28th Int. Electr. Power Distrib. Conf. (EPDC)*, IEEE, pp. 1–7, Apr. 2024, doi: 10.1109/epdc62178.2024.10571752.

[22] F. Alfaverh, M. Denai, and Y. Sun, "Optimal vehicle-to-grid control for supplementary frequency regulation using deep reinforcement learning," *Electr. Power Syst. Res.*, vol. 214, p. 108949, 2023.

[23] R. K. Khadanga, A. Kumar, and S. Panda, "Frequency control in hybrid distributed power systems via type-2 fuzzy PID controller," *IET Renew. Power Gener.*, vol. 15, no. 8, pp. 1706–1723, 2021.

[24] S. Shirali, S. Z. Moghaddam, and M. Aliasghary, "An interval type-2 fuzzy fractional-order PD-PI controller for frequency stabilization of islanded microgrids optimized with CO algorithm," *Int. J. Electr. Power Energy Syst.*, vol. 164, p. 110422, Mar. 2025, doi: 10.1016/j.ijepes.2024.110422.37.

[25] M. H. Khooban and M. Gheisarnejad, "A novel deep reinforcement learning controller-based type-II fuzzy system: Frequency regulation in microgrids," *IEEE Trans. Emerg. Topics Comput. Intell.*, vol. 5, no. 4, pp. 689–699, 2020.

[26] A. M. A. Soliman, M. B. Eldin, and M. A. Mehanna, "Application of WOA tuned type-2 FLC for LFC of two area power system with RFB and solar park considering TCPS in interline," *IEEE Access*, vol. 10, pp. 112007–112018, 2022.

[27] E. M. Ahmed *et al.*, "Frequency regulation of electric vehicle-penetrated power system using MPA-tuned new combined fractional order controllers," *IEEE Access*, vol. 9, pp. 107548–107565, 2021.

[28] A. Daraz *et al.*, "Optimized fractional order integral-tilt derivative controller for frequency regulation of interconnected diverse renewable energy resources," *IEEE Access*, vol. 10, pp. 43514–43527, 2022.

[29] A. Elmelegi *et al.*, "Optimized tilt fractional order cooperative controllers for preserving frequency stability in renewable energy-based power systems," *IEEE Access*, vol. 9, pp. 8261–8277, 2021.

[30] S. Shirali, H. Maleki, and H. Delavari, "A novel self-adaptive control for frequency stabilization in energy storage system with high penetration of renewable resources," in *Proc. 28th Int. Electr. Power Distrib. Conf. (EPDC)*, IEEE, pp. 1–7, Apr. 2024, doi: 10.1109/epdc62178.2024.10571695.

[31] E. Sahin, "Design of an optimized fractional high order differential feedback controller for load frequency control of a multi-area multi-source power system with nonlinearity," *IEEE Access*, vol. 8, pp. 12327–12342, 2020.

[32] S. Hu, W. Huang, N. Tai, J. Liu, L. Wang, and Y. Zhang, "Adaptive motor load control method for shipboard microgrid frequency regulation," *IEEE Trans. Transport. Electrific.*, 2024, doi: 10.1109/TTE.2024.XXXXXXX.

[33] D. J. Ryan, H. D. Torresan, R. Razzaghi, and B. Bahrani, "Frequency response of motor drive loads in microgrids," *IEEE Trans. Energy Convers.*, vol. 36, no. 2, pp. 1197–1206, 2020.

[34] H. Maleki, S. Shirali, H. Jamshidifar, and H. Delavari, "Enhanced obstacle avoidance of quadrotor UAV via fuzzy FOPID control and deep learning based observer," in *Proc. 10th Int. Conf. Control, Instrum. Autom. (ICCIA)*, IEEE, pp. 1–5, Nov. 2024, doi: 10.1109/iccia65044.2024.10768174.

[35] H. Maleki, S. Shirali, and H. Delavari, "Adaptive finite-time fractional order sliding mode controller with GMO optimization algorithm for inverted pendulum system," in *Proc. 10th Int. Conf. Control, Instrum. Autom. (ICCIA)*, IEEE, pp. 1–5, Nov. 2024, doi: 10.1109/iccia65044.2024.10768159.

[36] Shirali, S., Zolfaghari Moghaddam, S. , and Ali Asghary, M. "Load-Frequency Control of a Hybrid Islanded Microgrid with a Fractional Order Fuzzy PID Controller Optimized by Cheetah Algorithm", Journal of Modeling in Engineering, 22, 78, 2024, 217-231. doi: 10.22075/jme.2024.30979.2474 vol. 207, 114958, 2025.

[37] W. Younis, M. Z. Yameen, A. K. Junejo, et al., "Robust load frequency control in renewable integrated Multi Area grids using hybrid SA and QIO tuned PIDF controller," *Scientific Reports*, vol. 15, 36848, 2025.

[38] W. Zhao *et al.*, "Quadratic interpolation optimization (QIO): A new optimization algorithm based on generalized quadratic interpolation and its applications to real-world engineering problems," *Comput. Methods Appl. Mech. Eng.*, vol. 417, p. 116446, 2023.